Effects of porosity on drug release kinetics of swellable and erodible porous pharmaceutical solid dosage forms fabricated by hot melt droplet deposition 3D printing

Bin Zhang[1], Jehad Nasereddin[1,3], Thomas McDonagh[1], Didier von Zeppelin[4], Andy Gleadall[2], Fahad Alqahtani[1], Richard Bibb[5], Peter Belton[6], Sheng Qi[1*]

[1] School of Pharmacy, University of East Anglia, Norwich, NR4 7TJ, United Kingdom

[2] School of Mechanical, Electrical and Manufacturing Engineering, Loughborough University, Loughborough, LE11 3TU, UK

[3] Department of Pharmaceutical Sciences, Faculty of Pharmacy, Zarqa University, No 15 Damascus Highway, Zarqa, Jordan

[4]Arburg GmbH + Co KG, Germany

[5]School of Design & Creative Arts, Loughborough University, Loughborough, LE11 3TU, UK

[6] School of Chemistry, University of East Anglia, Norwich, NR4 7TJ, United Kingdom

Corresponding author: sheng.qi@uea.ac.uk

*Bin Zhang and Jehad Nasereddin are joint first authors.

Abstract

3D printing has the unique ability to produce porous pharmaceutical solid dosage forms on-demand. Although using porosity to alter drug release kinetics has been proposed in the literature, the effects of porosity on the swellable and erodible porous solid dosage forms have not been explored. This study used a model formulation containing hypromellose acetate succinate (HPMCAS), polyethylene oxide (PEO) and paracetamol and a newly developed hot melt droplet deposition 3D printing method, Arburg plastic free-forming (APF), to examine the porosity effects on *in vitro* drug release. This is the first study reporting the use of APF on 3D printing porous pharmaceutical tablets. With the unique pellet feeding mechanism of APF, it is important to explore its potential applications in pharmaceutical additive manufacturing. The pores were created by altering the infill percentages (%) of the APF printing between 20 to 100% to generate porous tablets. The printing quality of these porous tablets were examined. The APF printed formulation swelled in pH 1.2 HCl and eroded in pH 6.8 PBS. During the dissolution at pH 1.2, the swelling of the printing pathway led to the gradual decreases in the open pore area and complete closure of pores for the tablets with high infills. In pH 6.8 buffer media, the direct correlation between drug release rate and infills was observed for the tablets printed with infill at and less than 60%. The results revealed that drug release kinetics were controlled by the complex interplay of the porosity and dynamic changes of the tablets caused by swelling and erosion. It also implied the potential impact of fluid hydrodynamics on the in vitro data collection and interpretation of porous solids.

Keywords: Hot melt droplet deposition 3D printing, hot melt extrusion, Arburg plastic free-forming, controlled drug release, infill control, porous solids

1 Introduction

Pharmaceutical additive manufacturing is a field that has seen rapidly development in the past decade [1-4]. Material extrusion-based additive manufacturing (ME-AM) is one of the additive manufacturing methods that continues to attract increasing attention as a potential method to manufacture personalised pharmaceutical solid dosage forms [4-10]. The most reported thermal-based ME-AM operations in the pharmaceutical literature are hot melt filament-based extrusion printing (e.g. fused deposition modelling (FDM)) [1-11] and recently developed direct powder extrusion [12-15]. ME-AM allows for the rapid fabrication of highly tailored, bespoke objects with specific geometries that can fit the purpose of personalised medicines [16-22]. One process parameter which is often associated with its dose tailoring potential is the infill [23-29]. Sparse infill patterns are used in typical 3D printing to reduce material consumption and build time. The pattern and density of the infill can typically be specified in the printer control software when preparing a 3D print or it can be designed using 3D computer-aided design (CAD) software [30, 31]. When infill (%) is reduced, more free volume is created within a 3D printed object and porous structures can be created. In this study, a recently developed thermoplastic droplet deposition, Arburg Plastic Freeforming (APF) printing was used to produce porous tablets.

APF is a hot melt droplet-deposition printing that replicates some of the strengths of inkjet technology [32]. It deposits heated thermoplastic material via a piezo controlled nozzle that can open and shut-off at a defined frequency. The material deposition speed can be optimised by altering the frequency of the movement of the piezo. The droplets are deposited continuously to form a joined-up printing pathway, equivalent to the ones generated using hot melt filament-based extrusion printing (as illustrated in **Figure 1**).

In contrast to hot melt filament-based extrusion and APF is fed with granulated or pelletised materials instead of filaments. This overcomes the challenge for developing feedable and printable filaments that is faced by hot melt filament-based extrusion printing [33, 34]. In this study, the HME dispersions were pelletised and used as the feedstock for APF printing.

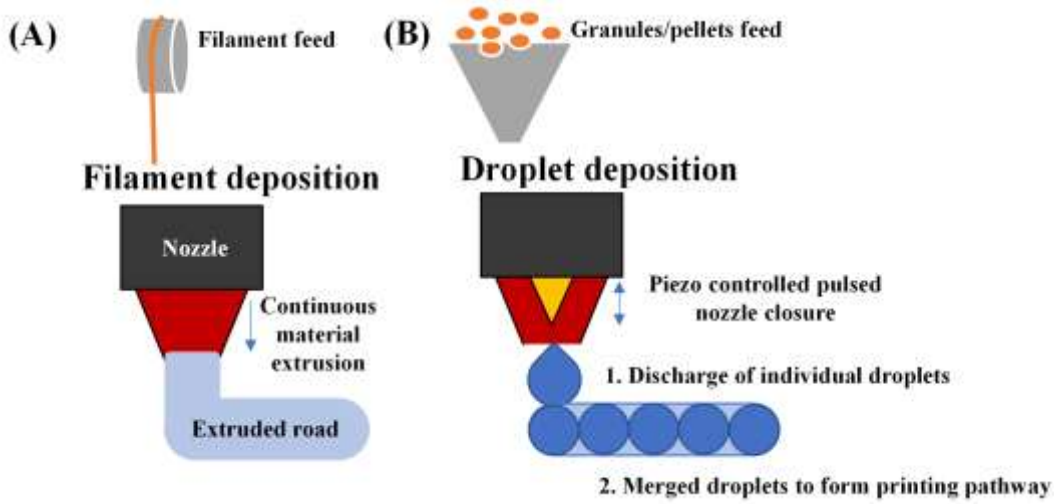

Figure 1. Illustration of two types of ME-AM deposition mechanism: (A) hot melt filament-based extrusion (i.e. FDM) and (B) hot melt droplet-based 3D printing (i.e. APF).

Infill, as a technical terminology, is often loosely used in the literature. In this study, infill is specifically referred to the amount of deposited material that occupies the internal part of a solid print that has a solid outer contour (sometimes called boundaries, perimeters or walls) but with open roof and floor (as illustrated in **Figure 2**). It is important to highlighted that the focus of this study is on the effect of microscale pores within the printed tablets, not the effects of the overall shape change of the tablets, on the drug release behaviour. Previously, other studies have concluded that for a non-porous 3D printed object, the drug release patterns are independent of the

shape/geometry designs of the object [23, 35]. The concept of reducing the infill to print porous solid dosage forms and to subsequently alter the drug release rate has been mostly explored in the literature for non-swellable and non-erodible materials with diffusion-controlled drug release [23-29]. The hypothesis behind this concept is that by implementing porous structures, such as the ones shown in **Figure 2**, the total surface area of the matrix exposed to solvents increases while maintain the overall outer dimensions.

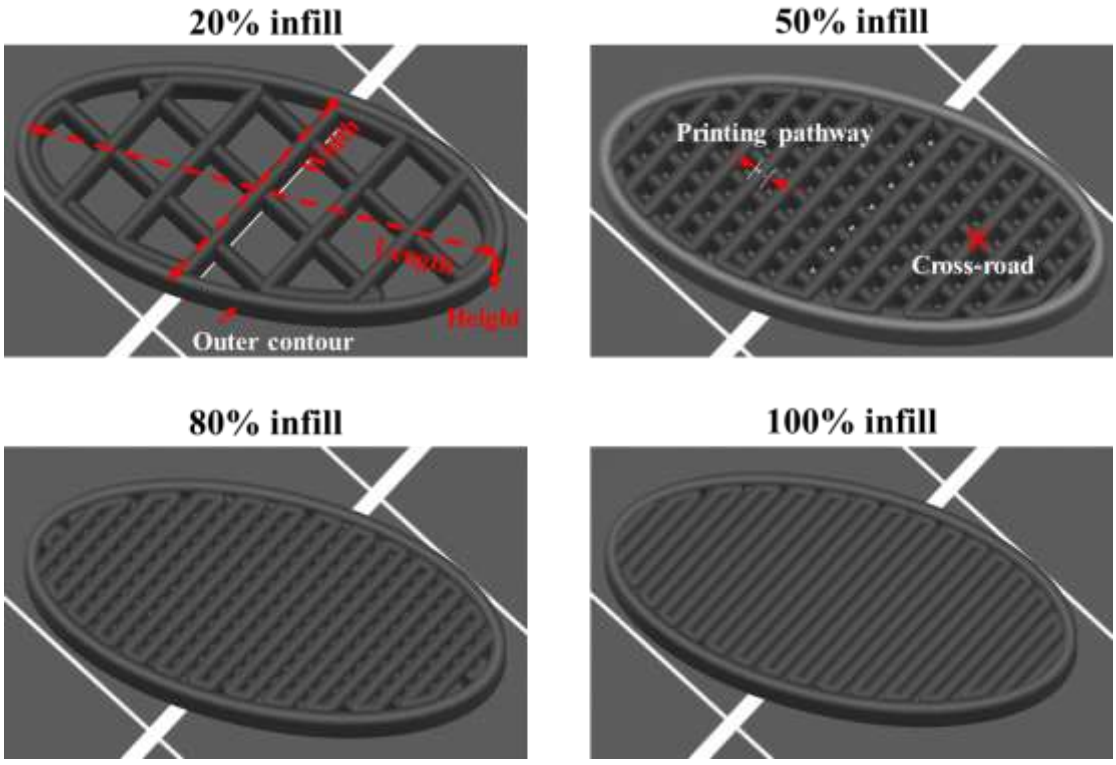

Figure 2. Illustration of the examples of the CAD designs of porous (with 20, 50, and 80% infill) and non-porous tablets (with 100% infill).

Concerning this concept, within the existing literature, proof-of-concept studies have been performed for two key milestones: (1) the printing of such porous solid dosage forms is achievable using both lipids and polymeric materials [24-29]; (2) a common finding of the level of porosity of the tablets can affect the drug release has been reached [24-29]. However, the knowledge gaps still exist in the following areas for using ME-AM

printing of porous solid dosage forms: (1) many literature on porous oral dosages were performed using thermoplastic polymers instead of pharmaceutical excipients used for oral administration and (2) most reported data are on drug release mechanisms dominated by diffusion in non-swellable and non-erodible materials. Most excipients and products used for oral administration go through erosion and swelling at some stage in the gut in the course of drug release. Therefore, it is important to gain a fuller understanding of swellable and erodible 3D printed porous dosage forms. This study used a blend of hypromellose acetate succinate (HPMCAS) and polyethylene oxide (PEO) as the base of the solid dispersion. HPMCAS, PEG and PEO have been used for hot melt extrusion-coupled FDM printing in other reported studies to produce solid oral dosage forms (printed with 100% infill) with various geometries [17, 28, 35-38], but with no micron-scaled porosity. HPMCAS is only soluble above pH 5 [39]. The formulation swells in pH 1.2 HCl due to the presence of PEO and erodes in pH 6.8 PBS, thus can act as a model swellable material and an erodible material by changing the pH of the dissolution media.

With the use of the model system, this study aimed to examine two specific areas, the printing quality of APF and whether specified porosity can be used to control drug release for swellable and erodible materials. In the literature, printing quality is typically judged on measurements of weight and drug content uniformity compared to pharmacopeial standards and reproducibility of the outer dimensions of the hot melt filament-based extrusion printed tablets [19, 29, 40]. In most cases, the 3D printing tablets met weight uniformity specifications, indicating that the printing of tablets with the same design is reproducible. However, for porous tablets with micron-scale structures there is no measure developed or proposed to examine the printing quality with different infills. As the inner printing pathway are exposed, and are therefore surfaces

for drug release, the uniformity of the printing pathway widths could have a significant impact on the reproducibility of the subsequent drug release performance of the porous printed tablets. The data in the literature show that most porous tablets printed by hot melt filament-based extrusion printers have certain levels of micron-scale defects at the individual printing pathway level [19, 23-29, 40-43]. This may be related to the continuous printing pathway-laying nature of the material deposition of these printers, which makes the printing pathway turning point and layer-overlapping points extremely challenging to produce repeatably and defect-free, and highly dependent on the thermal viscoelastic properties of the materials [40, 42, 43]. With the droplet deposition nature, APF may be able to reduce these issues as the printing pathway are formed by merging individual droplets instead of the continuous extrusion and stretching of molten material. This was examined within this study.

In terms of the porosity controlling drug release, early literature on 3D printed porous tablets used a solid roof and floor with a porous interior, probably due to using available software options to specify percentage infill [24, 28]. This made the evaluation of the effects of porosity on drug release inconclusive because the tablets did not have open porosity. For example, work by Lamichhane and co-workers' showed no significant difference in drug release rate between the formulations with different infills in samples with solid roofs; whereas with prints having an open roof and floor, the effect of infill on drug release can be clearly seen, but the trend is complex [28]. When the qualities of the prints were examined, poor print quality may have been of the cause of poor reproducibility of the porosity and subsequently the inconsistency of the drug release results. However Isreb and co-workers data on the FDM printed 'radiator-like' tablets using PEG and PEO demonstrated the effects of spacings between layers on the drug release kinetics [37]. With higher printing quality of micro-scale structural details using

melt inkjet printing, Kyobula and co-worker's confirmed that infill was one of the key factors affecting the drug release of fenofibrate-loaded beeswax tablets [27]. This study reported no observed swelling or erosion from the porous tablets during dissolution, making the release mechanism entirely diffusion based. Of the six infills investigated, the four lower infill formulations showed no significant differences in drug release but were significantly faster than a higher infill formulation, and the 100% infill formulation [27]. In practice, many pharmaceutical solid dispersions are swellable and erodible. Therefore, it is important to understand the behaviour of this group of materials when they are used to produce 3D printed solid dosage forms.

2 Materials and Methods

2.1 Materials

Hypromellose acetate succinate (HPMCAS, low-fine grade) was kindly donated by Shin Etsu (Shin Etsu Inc., Tokyo, Japan). Polyethylene oxide N-10 grade (PEO; molecular weight of 100,000) was kindly donated by Colorcon (Colorcon Ltd., Dartford, United Kingdom). Paracetamol (PAC) was purchased from Sigma Aldrich (Sigma Aldrich, Salisbury, United Kingdom).

2.2 Preparation of filaments by hot melt extrusion (HME)

Filaments were prepared to the weight ratio of 81% HPMCAS, 10% PAC, and 9% PEO using a Haake Minilab II hot melt compounder (Thermo Scientific, Karlsruhe, Germany) equipped with a 1.75 mm circular die. Extrusion was conducted at a screw speed of 100 RPM and a temperature of 155 °C. Materials were cycled in the extruder for 5 minutes prior to flushing to ensure homogeneity along the filament. The melt was flushed at a screw speed of 35 RPM onto a conveyer belt. To achieve a wide range of

filament diameters for drug release tests (from 20 μm to 1.75 mm), the filament described above was feed through a RepRap x400 3D printing system and 'drawn' from the nozzle at different speeds by manually rotating and moving a mandrel by hand. After 'drawing', the filament diameter was measured with a digital vernier calliper along its length to identify regions of consistent and appropriate diameters (approximately 20 μm, 350 μm, 650 μm and 1.8 mm), and these sections were cut away as small length (10 mm) for drug release tests. The diameters of tested filaments were accurately measured prior to the dissolution test using a digital vernier calliper.

2.3 HME pellets preparation and APF printing of tablets

The pellets used for APF printing were produced using a larger scale extruder, Pharma 16 twin-screw extruder (ThermoFisher Scientific, UK), than the one used in 2.2. This is due to the larger batch volume of the pellets required for the feeding of the APF printer. The extruder was coupled with a using a VariCut 16 Strand Pelletiser (Thermofisher Scientific, UK). The extrudates were produced at 150°C and 100 rpm using a circular die of 1.75 mm diameter. The extruded strands were guided onto a conveyer belt and collected continuously and cut into pellets at averagely 3 mm in length the pelletiser.

Prior to the tablet printing, the feeding hopper of the APF printer (Freeformer®, Arburg, Germany) was filled with HPMCAS-PEO-PAC pellets prepared by HEM. The following temperature profile was used for the tablet printing: discharge nozzle, 170°C; barrel zone 2, 120°C; barrel zone 1, 93°C. In order to achieve 0.20 mm droplet layer height, the discharge value of 45% and the droplets aspect ratio (width/height) of 1.005 was set. The defined elliptical tablets geometry (8×15×3 mm) with variable infilling density ranging from 20% to 100% were printed. The printing operation and the CAD

file uploading were controlled through the APF operational interface integrated within the printer.

2.4 Differential scanning calorimetry (DSC)

The thermal properties of the raw polymers, the physical mixtures, the HME extrudates/pellets and the printed tablets were characterised using a Q20 differential scanning calorimetry (DSC) (TA Instruments, Delaware, United States). The DSC was calibrated prior to samples measurement. Each sample (3-5 mg) was accurately weighed in an aluminium crimped DSC pan (TA Instruments, Delaware, United States) with a lid. All samples were tested at a 5°C/min scanning rate. Nitrogen purge gas with a flow rate of 50 mL/min was used throughout the experiments. TA Universal Analysis 2000 software was used for the data analysis. All tests were performed in triplicates.

2.5 Attenuated total reflectance-Fourier transform infrared spectroscopy (ATR-FTIR)

ATR-FTIR measurements were conducted using a Vertex 70 FTIR spectrometer (Bruker Optics Ltd., United Kingdom), equipped with a Golden Gate, heat-enabled Attenuated Total Reflectance (ATR) accessory (Specac Ltd., Orpington, United Kingdom) fitted with a diamond internal reflection element. ATR-FTIR spectra were acquired in absorbance mode, using a resolution of 4 cm^{-1}, 32 scans for each sample, within the range of wavenumbers from 4000 cm^{-1} to 650 cm^{-1}. Spectra analysis was conducted using OPUS version 7.8 (Bruker Optics Ltd., United Kingdom). All measurements were done in triplicate.

2.6 Powder X-Ray diffraction (PXRD)

A D5005 X-ray diffractometer (Siemens, Munich, Germany) with monochromatic CuKα radiation (wavelength =1.54056 Å) was used to measure the raw materials, the physical mixtures, the extrudates and the APF printed tablets. The extrudates and the printed tablets were briefly grinded to powder form prior to their measurements. The samples were scanned from a 2θ angle of 5° to 50°, with a scan speed of 2°/min. The scan step was maintained at 0.02°, the resultant scan resolution was found to be 0.0025.

2.7 Swelling tests

The swelling experiments were performed on the APF printed tablet. The tablets were immersed in 900 mL of pH 1.2 media at 37 °C in a USP paddle apparatus with a rotating speed of 50 rpm. At each 30 minutes, samples were removed and imaged using a Linkam Imaging Station (Linkam Scientific Instruments, Tadworth, United Kingdom). The printing pathway and pore area were quantified by measuring 10 times in Image J software (http://rsb.info.nih.gov/ij/); the data was exported for analysis, and the statistical distributions were plotted using Origin software (OriginLab, USA).

2.8 *In vitro* drug release studies

Two dissolution media were used, pH 1.2 HCl and pH 6.8 buffer. The pH 1.2 HCl medium was prepared by adding 100 mL of 1 M HCl solution into 1000 mL Milli-Q water and stirring until it completely mixing. For the pH 6.8 buffer medium, 6.8 g of monobasic potassium phosphate (KH_2PO_4) was dissolved in Milli-Q water and diluted with water to 1000 mL volumetric flask then stirring for at least 3 hours to make sure KH_2PO_4 completely dissolved. 0.9 g of sodium hydroxide (NaOH) was then added into the solution and stirred for 3 hours until completely dissolved. The pH of the result

222 solution was measured using a pH meter (Hanna Instruments, Padova, Italy) and
223 adjusted (if required) to 6.8.

224 *In vitro* drug release of the HME filaments with different diameters were performed
225 using a shaking incubator (IKA KS3000i, Staufen, Germany) with 100 rpm at 37 °C.
226 The samples were measured accurately for weight and placed in glass vials with 20 mL
227 pH 1.2 or pH 6.8 media that were pre-heated to 37 °C. The time point for HME filament
228 in pH 1.2 and 6.8 media was 5, 10, 15, 30, 45, 60, 120, 180, 240, 420, 720 and 1560
229 minutes. 2 mL aliquot was withdrawn at each time point and replaced with pre-heated
230 fresh media.

231 A Caleva 8ST USP paddle dissolution apparatus (Caleva Ltd., Dorset, United
232 Kingdom) was used to test the APF printed tablets in 900 mL dissolution media either
233 at pH 1.2 or pH 6.8 with 50 rpm paddle rotation rate and at 37± 0.5 ºC. 5 mL aliquots
234 were withdrawn from the dissolution media at predetermined time points and replaced
235 with 5 mL of preheated fresh dissolution media. The time points for the APF tablets in
236 pH 1.2 buffer were 30, 60, 120, 240, 330, 480, 1200 and 1560 minutes. Considering the
237 APF tablets having faster dissolution in pH 6.8 buffer than in pH 1.2 buffer due to the
238 HPMCAS being soluble at pH 6.8, shorter total dissolution periods and more sampling
239 time points within the 1st hour were used, which was 5, 10, 15, 30, 45, 60, 165, 300 and
240 600 minutes. All APF tablets with variable infill were fully dissolved in pH 6.8 buffer
241 within 2 hours. Drug content was analysed using a UV-Visible spectrophotometer
242 (Perkin-Elmer lambda 35, USA) at a wavelength of 242 nm. At least three samples
243 from each formulation were tested.

2.9 *In vitro* drug release data analysis

As the hot melt extrudates are close to an ideal cylindrical in shape, and if it is assumed that the dissolution rate is determined by Fick type I diffusion from the filament, which is semi-infinite, then the rate may be modelled by using the solution to the diffusion equation for a cylinder which is:

$$\frac{M_t}{M_0} = 1 - \sum_{n=1}^{\infty} \frac{4}{a^2\alpha^2} exp^{(-D\alpha^2 t)} \quad \text{Equation 1}$$

where $(a\alpha)_n$ are the roots of the zero order Bessel function, a is the radius of the cylinder and D is the diffusion coefficient, t is time. In addition, drug release data of APF tablets were fitted to a single exponential model, as shown below:

$$\frac{M_t}{M_0} = A\left(1 - \exp\left(-\frac{t}{T}\right)\right) \quad \text{Equation 2}$$

where M_t is the mass of drug released at time t, M_0 is the total mass of drug in the sample, A is the fitting factor that represents the fraction of m_0 actually released at $t = \infty$, T is time constant.

3 Results and discussion

3.1 Formulation characterisation

Figure 3A shows the DSC thermograms of the raw materials, physical mixtures and the filaments prepared by HME and the APF printed tablet. For the raw materials, the T_g of HPMCAS is seen at ~120 °C. An endothermic event corresponding to the T_m of PEO is seen at 60 ± 1.1 °C. The melting (T_m) of PAC form I (monoclinic form) was seen at ~169 ± 0.79 °C which agrees well with the literature [44]. For the physical mixture, the both T_m of the crystalline fraction of PEO and the T_m of crystalline PAC

are clearly visible (**Figure 3B**). No visible melting of PAC can be observed in the DSC results of the hot melt extrudate and APF printed tablet. With 10% PAC loading, the crystalline PAC can be detected using ATR-FTIR and PXRD in the physical mixtures (**Figure 3C and 3E**). As seen in **Figure 3C**, there is notable broadening of the N-H stretching peak of crystalline PAC at 3321 cm^{-1} indicating the significant loss of crystallinity. The peak at 808 cm^{-1}, representing the out-of-plane bending of a para-substituted aromatic ring of PAC that is particularly indicative of the crystal packing of the monoclinic form of PAC [45], is absent in the spectra of the HME filament and the APF printed (**Figure 3D**). The halo shaped PXRD diffraction patterns of the filaments and the APF printed tablet showed no PAC crystalline peaks. The DSC, PXRD and ATR-FTIR data are in good agreement of the formation of amorphous dispersion of PAC in the HPMCAS-PEO matrix.

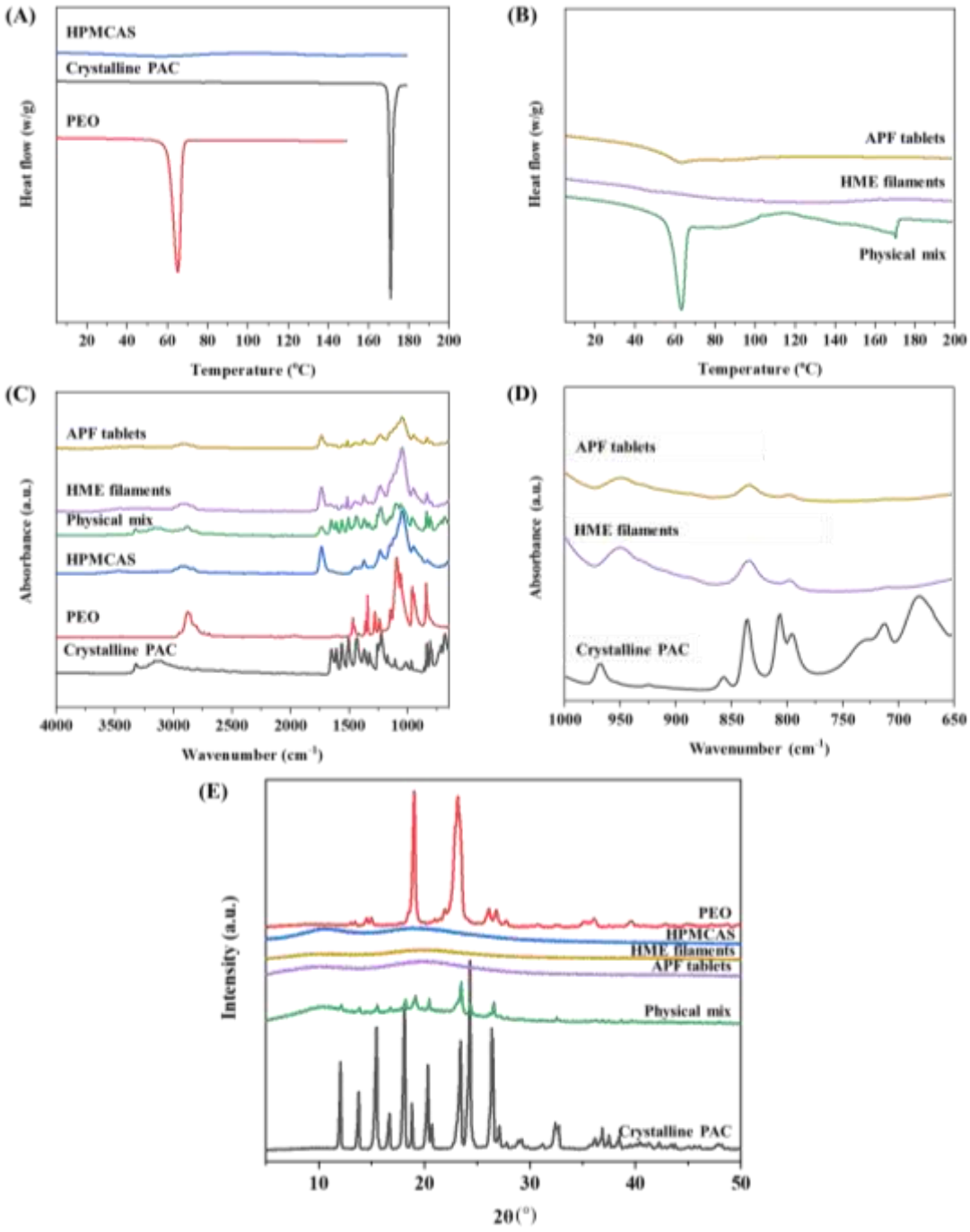

277

278 **Figure 3**. DSC thermograms of (A) the raw materials and (B) the physical mix, the

279 HME filaments and the APF tablets; (C) ATR-FTIR spectra of the raw materials, the

280 HME filaments and the APF tablets; (D) ATR-FTIR spectra of crystalline PAC and the

281 HME-filaments, showing the disappearance of the 808 cm^{-1} aromatic CH bending peak;

(E) PXRD diffraction patterns of the raw materials, the physical mix, the HME filaments and the APF tablets.

3.2 Evaluation of the printing quality of the porous tablets prepared by APF

Figure 4A shows the detailed morphologies of the APF printed porous tablets with tablets with 20%, 50% and 80% infills as examples tested using SEM. Clear defects (i.e. mis-aligned outer contour) can be seen in the tablets with 20% infill. A unique feature of the widths of the printing pathways at the cross-roads being wider than the rest of 'free-handing' printing pathways is observed. The cause of this is uncertain, but it could be due to droplet deposition nature of the APF printing. The pore area (i.e. the surface area of the interfilamentous gap area) was not measurable for the tablet with 80% infill as the pores were too small to be accurately measured. The analysis of the pore area of the APF printed tablets with 20-70% infill is summarised in **Figure 4B**. The results of the APF printed tablets with 20-70% infill indicate the mean pore area has a power law relationship with the infill. This is in close agreement with the theoretical calculation of the pore area using the CAD file designs of the tablets (red dots in Figure 4B).

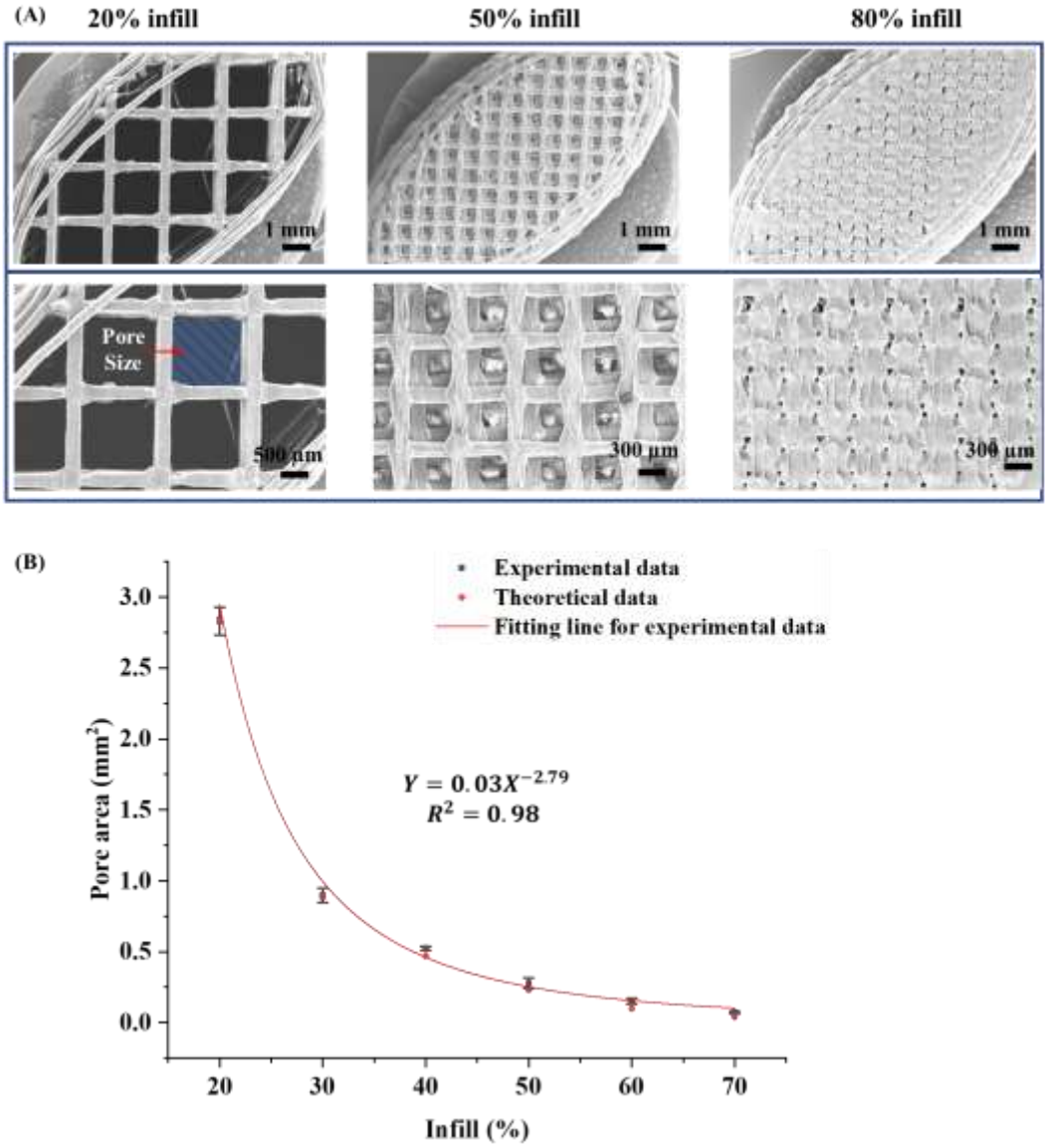

299

300 **Figure 4**. (A) SEM image of APF printed tablets with 20%, 50% and 80% infills, and
301 (B) the measurement of pore area (void space between printing pathways as illustrated
302 in A) of the APF printed tablets with infills between 20-70%.

303 The uniformities of the outer dimensions (height, width, and length) and the weight of
304 APF printed tablets with 20-100% infills are summarised in the **Table 1**. The inter-
305 tablet variations of the outer dimension (height, width, and length) of the APF printed
306 tablets are less than 1, 0.7 and 2 % in width, length and height, respectively. The
307 detailed inspection of each dimensional parameters of the APF printed tablets revealed

that they are all closely resemble the dimensions of the CAD elliptical design (8×15×3 mm) with less than 0.4 mm deviation. The uniformity data of the outer dimension of the APF printed tablets implies the high reproducibility of the APF printing for the geometry control.

Table 1. Outer dimension and weight uniformity of the APF printed tablets. The dimension of the elliptical tablets CAD model is 8 (width)×15 (length) ×3 (height) mm (n=3).

Infill (%)	Width (mm)	Length (mm)	Height (mm)	Weight (mg)
20	8.03±0.06	14.60±0.10	2.90±0.03	78.3±2.5
30	8.02±0.06	14.86±0.08	2.92±0.03	114.4±2.8
40	8.03±0.08	14.86±0.04	2.97±0.02	140.6±3.3
50	8.02±0.02	14.89±0.02	2.97±0.01	166.5±7.6
60	8.01±0.02	14.87±0.03	2.98±0.06	198.7±8.2
70	8.02±0.06	14.87±0.04	2.95±0.03	230.7±5.4
80	7.96±0.07	14.92±0.04	2.96±0.04	260.9±8.5
90	7.97±0.02	14.89±0.05	2.98±0.01	288.2±5.5
100	7.93±0.06	14.86±0.05	3.03±0.02	300.9±1.0

There is no clear trend of the weight variation being associated with infill used for printing. The weight uniformity of the APF printed tablets are all within the pharmacopeial specification of mass uniformity for tablets (>80 mg, 80-250 mg and <250mg categories) and are comparable with the variabilities reported in the literature of the tablets printed using FDM [28, 29, 37]. The highly linear correlation between the infill and the tablet weight of the APF printed tablets is demonstrated by the R^2 of 0.9951 (**Figure 5A**). This indicates the APF has good control of consistency of material deposition during the printing process. As all tablets were printed with the same

numbers of layers, the intercept of 27.213 mg obtained from the linear fitting is the weight of the unchanged outer contour for all the tablets with different infills.

As revealed by the SEM images of the APF tablets (**Figure 4A**), the width of the printing pathway at the cross-road is wider than the rest. Therefore, the analysis of the uniformity of the width of the printing pathway of the APF printed tablets was performed. As seen in **Figure 5 B**, no significant difference in the width of the printing pathways at different locations of the tablets with low infill (20%), whereas the tablets with higher infills (50 and 80%) the width at the cross-road are significantly higher than the rest of the tablets. Currently it is unclear if this particular feature would impact on the drug release behaviour and require further investigation which is out of the scope of this study. However, with the dimension and weight uniformity data, it is clear that this feature is not affecting the macroscopic level of the properties of the tablets.

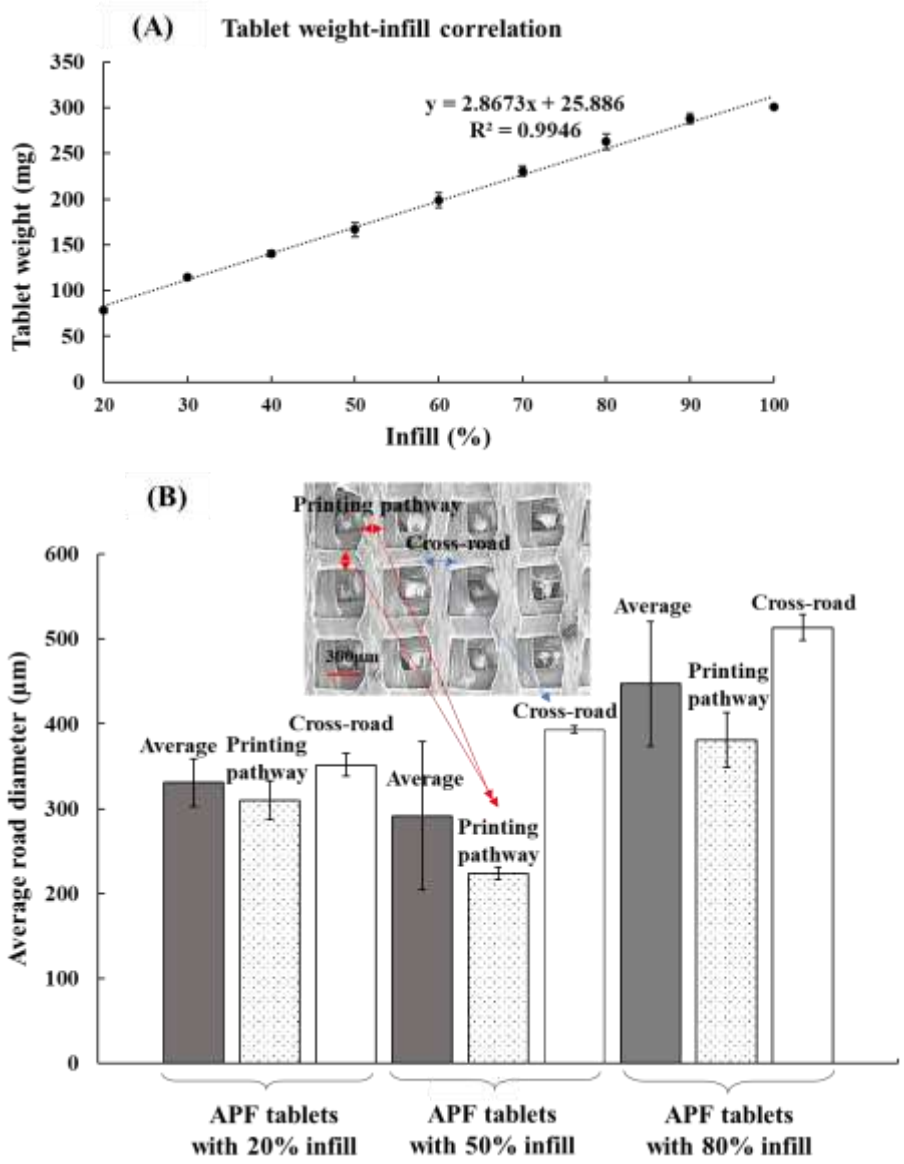

337

338 **Figure 5**. (A) The relationship between the infilling density and the weight of APF
339 printed tablet, and (B) the printing pathway width uniformity of APF printed porous
340 tablets with different infills. The insert image is the SEM images of APF printed tablets
341 with 50% infill (labelled with the illustrations of the data population named as 'printing
342 pathway' and 'cross-road').

343

3.3 *In vitro* drug release of drug-loaded HME filaments

In order to examine the hypothesis that porosity and infill can be used to manipulate the drug release from porous tablet, the drug release of the simplest two-dimensional filaments with diameters ranging from approximately 20 µm to 1.8 mm were tested. As the filaments are simple cylinders, changing the diameter of the filament changes both the overall surface area and volume of the samples. As weights of all tested filaments were kept as closely similar as possible, the surface area per unit mass of the filaments ranges from 2 to 38 mm^2/mg. As seen in **Figure 6**, the drug release rate of the filaments with smallest diameter released drug fastest in both pH 1.2 and 6.8 media. HPMCAS being insoluble at pH 1.2, thus the drug release rate in pH 1.2 is significantly slower than in pH 6.8 media, in which HPMCAS became soluble.

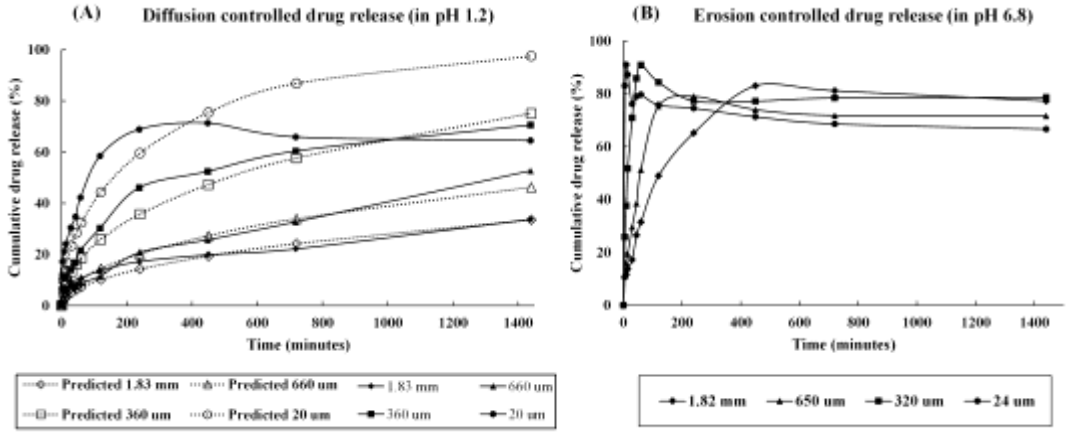

Figure 6. *In vitro* drug release of HME filaments with a range of diameters (A) in pH 1.2 and (B) in pH 6.8 buffer media. Note: the dotted line in A is not fitted line of the drug release data of the filaments, but the predicted drug release if assuming the filaments are ideal cylinders and the drug release profiles follow a simple diffusion model.

The dotted lines in **Figure 6A** show the predicted curves obtained assuming that the diffusion coefficient (D) of drug, $6.7x10^{-14}$ m^2/s. This value was calculated from the simulation based on **Equation 1** that gave curves on the same time scale as the observed experimental release drug profiles. It should be emphasised that the curves in the figure are not attempts at best fit to the data but hypothetical curves that would be observed if the simple diffusion model applied. The difference seen between the predicted results and the experimental (**Figure 6A**) may be attributed to a number of factors: (1) Although the width to length ratio of the filaments is small, the assumption of the semi-infinite model may not be correct; (2) thin filaments flexed/coiled during the drug release process and this changed geometry; (3) although HPMCAS is not soluble at pH 1.2, PEO is a highly swellable material. This led to a degree of swelling of the filaments in pH 1.2.

In pH 6.8 media, in which HPMCAS becomes soluble and the filaments erode, the drug release from the filaments are significantly faster (**Figure 6B**). The diameter of the filament still shows a clear impact on the drug kinetics. The filament with the smallest diameter (24 μm) rapidly dissolved and released drug within less than 5 minutes; whereas the filaments with the largest diameter (1.82 mm) less than 50% of the drug load in 180 minutes. These results implied the clear correlation between SA and drug release for both erosion (in pH 6.8) and swellable (in pH 1.2) systems.

To summarise, the results show that the *in vitro* drug release rates in both pH 1.2 and pH 6.8 depend on the radius of deposited filaments. When this is translated into the cases of APF printed multi-printing pathway tablets, the implication is that if the printing pathway width is kept constant, increasing the number of printing pathways (different infills) should not change the relative drug release rate. In this case any effect

of infill seen, if printing pathway radius is kept constant, will be due to the change in space between the printing pathways. This is further tested on the APF printed tablets.

3.4 Effects of porosity on *in vitro* drug release of swellable porous tablets

The swellability of the APF printed tablets in pH 1.2 media was examined prior to the drug release test in order to evaluate the extent of the swelling of the printing pathway and assess their possible effect on the pore area during dissolution. As HPMCAS is soluble at pH 6.8, the APF printed tablet was dissolved within the pH 6.8 medium; thus the swelling test was only performed at pH 1.2. As seen in **Figure 7A and 7B**, the printed printing pathways show clear evidence of swelling in pH 1.2 medium. The example tablet with 60% infill shows continuous swelling of the printing pathways. This led to the reduction of the pore area with time (**Figure 7C**). Such a change in printing pathway width would dynamically impact on the SA of the tablet during the dissolution process. As swelling occurs, the diffusion coefficient of the drug from the matrix is likely to change and the diffusion pathway from the interior of the printing pathway will increase. At the same time the pore dimensions will be reduced. For the tablets with high infill levels, due to the swelling of the printing pathways, the size of the pores created by the infill could reduce significantly. These tablets have lower spatial allowances (smaller pores) to accommodate swelling than the tablets with lower infills, therefore, the pores get filled up more quickly than the tablets with lower infills, which limits the drug release. These mechanisms led to the prediction of drug release kinetics of a swellable system being complex to resolve.

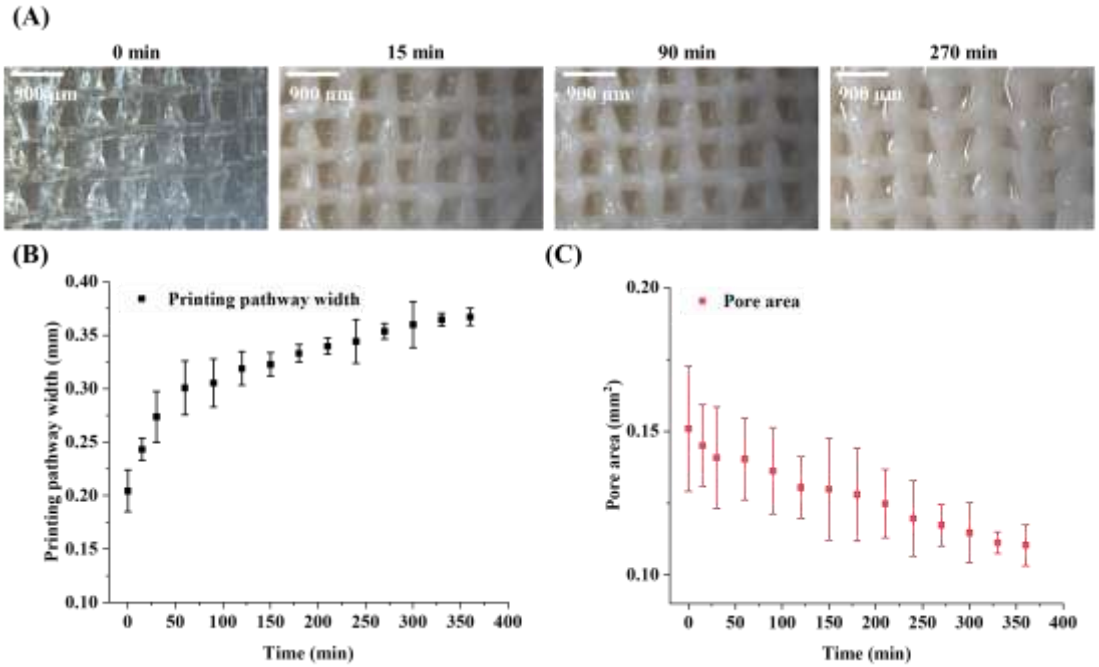

Figure 7. (A) Example microscopic images evidencing the swelling of APF printed tablet with 60% infill in pH 1.2 HCl at the time points of 0, 15, 90 and 270 minutes; (B) printing pathway width and (C) pore area measured at time point in the pH 1.2 HCl.

The *in vitro* dissolution data of the APF printed tablets in pH 1.2 HCl revealed slower drug release rates, with the 30% infill tablets have the significantly fastest drug release among all tested tablets (**Figure 8A**). The tablets with 60% infill released drug significantly faster than the ones with 100% infill. The drug release rate increasing with decreasing infill agrees with the correlation of SA/V and drug release kinetics [23, 27, 32]. The difference in the drug release rates between the tablets with 90 and 100% infills is insignificant (see **Supplementary Materials Figure S1**). Due to the swelling of the printing pathways, this can be attributed to the blockage of the pores within the 90% density tablets. Moreover, the results highlight that when designing a 3D printed solid dosage form from swellable material, it is important to fully understand the swelling behaviour which can be used to guide the geometry design of the dosage form in order

to achieve desired drug release pattern. In practical terms the pore size must exceed the swelling.

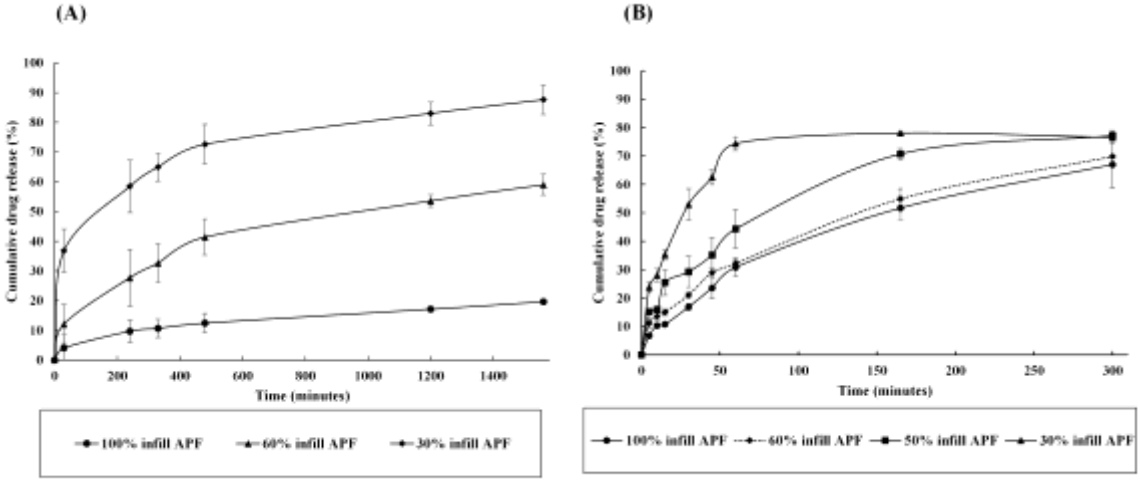

Figure 8. *In vitro* dissolution results of the APF printed tablets in (A) pH 1.2 HCl and (B) pH 6.8 buffer media.

3.5 Effects of porosity on in vitro drug release of erodible porous tablets

As APF allowed the printing of tablets with 10% infill interval, the effect of infill on the drug release can be investigated in more detail. The full set of the dissolution data of the APF printed tablets can be found in the Supplementary Materials (**Figure S2**). For the tablets with infills between 20-50%, the drug release rates increase with decreasing the tablet infill, which could be attributed to the SA/V difference. However, the drug release rate of the APF printed tablets with 60-100% infills show no significant difference between them (**Figure 8B**). This may seem to be in contradiction with the SA/V hypothesis. However, if the pores are sufficiently small, the entrapments of air within the pores may delay the wetting of the tablets and reduce the drug release rate [27]. This is also observed by the Kyobula and co-worker in their study on the thermal inkjet-printed beeswax tablets with honeycomb pores [27]. These results highlight that

governing drug release by altering SA/V is much more complex in practice and multiple material and surface properties of the prints should be thoroughly examined and taken into consideration during the microstructure design of the porous tablets.

The drug release data of the APF tablet with the infill from 20 to 100% were fitting with the exponential model described using **Equation 2**. The fitting parameters were summarised in the **Table 2** (fitting details can be found in Supplementary Materials **Figure S3**). The time constant *T* shows clear linear correlation with the infill (**Figure 9 (A)**) for the tablets with 100%, and 20-50% infills. This result indicates the direct correlation between the drug release rate and infill. As seen in **Figure 9 (B)**, this linear correlation is weakened when the results of the tablets with 60-90% infills were added. This agrees well with the insignificant difference in the *in vitro* drug release data of these tablets with infills between 60-100%. As indicated earlier, this could be due to the swelling prior to erosion of the printing pathways within these tablets, which led to the differences in pore area of these tablets being negligible (i.e. the pores become closed).

Table 2. Fitting parameters of the *in vitro* drug release data of the APF tablets in pH 6.8 buffer medium.

Infilling (%)	A	T (minutes)	R^2
20	81.5	12.4	0.987
30	77.0	23.2	0.979
40	75.5	30.0	0.980
50	76.0	60.6	0.953
60	68.6	83.7	0.966
70	61.8	107.7	0.949
80	82.74	141.9	0.984

90	67.0	112.5	0.977
100	69.2	105.1	0.987

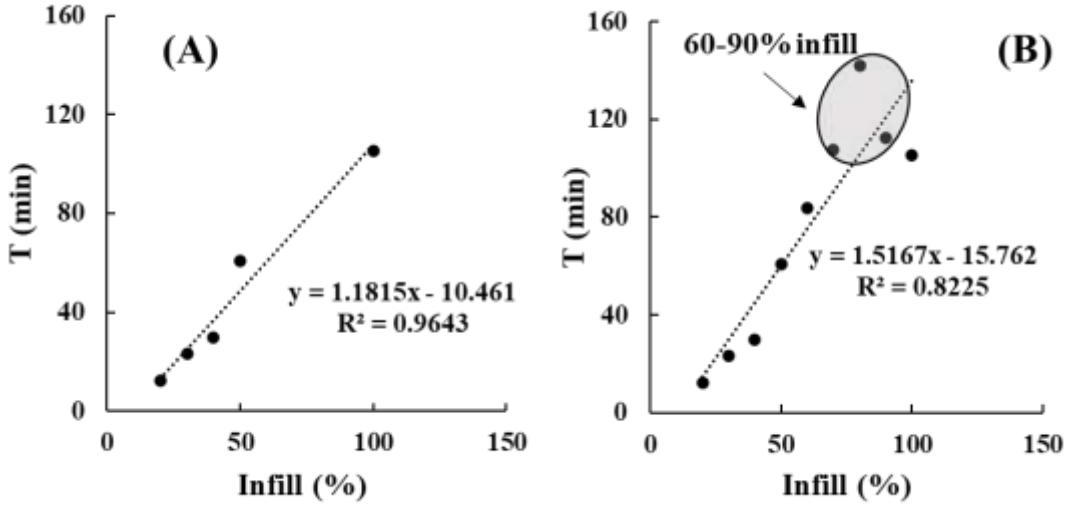

Figure 9. (A) The linear correlation between the time constant T and infill for the tablets with 100, and 20-50% infills; (B) linear correlation is weakened when the results of the tablets with 60-90% infills were added.

It is also worth mentioning that high standard deviations are often seen in the *in vitro* drug release results of 3D printing porous tablet [23-25, 46]. When interpreting and comparing *in vitro* drug release data between formulations, the effects of fluid dynamics created by the *in vitro* dissolution testing methods are often not discussed but should be taken into consideration. In the literature, both paddle [23, 24, 27, 28] and basket [25, 29] methods were used. D'Arcy and co-workers' computational fluid dynamic study revealed that the velocities of the flow field solution within the basket (USP Apparatus 1) to be of the same order as those at the base of the paddle apparatus (USP Apparatus 2) at the same rotation speed and should provide equivalent dissolution rate data if the solid dosage forms were placed either in the basket or at the bottom of the vessel for

paddle method [47]. Therefore, in theory, the method for dissolution should not affect the reproducibility of the results. However, most porous tablets, particularly the ones with low infills, have a strong tendency to float when the paddle method was used. Literature data also showed that floating during dissolution led to higher standard deviation of the result [28]. This is confirmed by hydrodynamic studies performed by D'Arcy and co-workers demonstrating less variability in dissolution data from tablets fixed to a single position compared with those that were not fixed [46, 48]. For porous tablets that float during dissolution, using basket method, in our case, did not improve the reproducibility of the *in vitro* release data (as seen in **Supplementary Materials Figure S4**). The differences observed between the drug release data obtained by paddle and basket method suggest the hydrodynamics within the dissolution bath can significantly affect the drug release rate of the tested dosage from in particular for porous tablets. It is clear that both hydrodynamic effects and the role of air entrapment in release dynamics is likely to be an important factor in understanding drug release kinetics but was beyond the scope of this study.

4 Conclusion

The results of this study indicates that APF can be used to reproducibly 3D print porous tablets using pharmaceutical polymers, such as HPMCAS and PEO, and can produce tablets with a wide range of infills. Although using porosity to control the drug release in diffusion-controlled systems is well-documented, there was no detailed study on whether porosity can be used for drug release control of swellable and erodible systems. The results of this study for the first time indicates that there is a linear correlation between the drug release rate constant and infill when pore size is not affected significantly by swelling. This suggests that porosity may be used to control drug

release rate in swellable and erodible systems. However, the control over the absolute value of the drug release rate is much more complex than just the infill. It is an interplay between the swelling/erosion kinetics, surface properties, and the hydrodynamic of the flow during the *in vitro* testing.

Acknowledgement:

We would like to thank the Enabling Innovation: Research to Application (EIRA), a Research England Connecting Capability Fund (CCF) project for providing the funding for the study. We would like to thank Prof Dennis Douroumis and his team, Dr. Steven Ross, Mr Md Sadeque Hossain Mithu and Mr Atabak Ghanizadeh Tabriz at the Faculty of Engineering and Science of University of Greenwich for their assistance in the preparation of the hot melt extruded pellets.

References

1. Awad A, Trenfield SJ, Gaisford S, Basit AW. **3D printed medicines: A new branch of digital healthcare**. *International journal of pharmaceutics* 2018; 548(1):586-596.
2. Madla CM, Trenfield SJ, Goyanes A, Gaisford S, Basit AW. **3D printing technologies, implementation and regulation: An overview**. *3D printing of pharmaceuticals* 2018:21-40.
3. Basit AW, Gaisford S. **3D printing of pharmaceuticals**. Springer; 2018.
4. Trenfield SJ, Awad A, Goyanes A, Gaisford S, Basit AW. **3D printing pharmaceuticals: drug development to frontline care**. *Trends in pharmacological sciences* 2018; 39(5):440-451.
5. Katstra W, Palazzolo R, Rowe C, Giritlioglu B, Teung P, Cima M. **Oral dosage forms fabricated by Three Dimensional Printing™**. *Journal of controlled release* 2000; 66(1):1-9.
6. Alomari M, Mohamed FH, Basit AW, Gaisford S. **Personalised dosing: printing a dose of one's own medicine**. *International journal of pharmaceutics* 2015; 494(2):568-577.
7. Alhnan MA, Okwuosa TC, Sadia M, Wan K-W, Ahmed W, Arafat B. **Emergence of 3D printed dosage forms: opportunities and challenges**. *Pharmaceutical research* 2016; 33(8):1817-1832.
8. Norman J, Madurawe RD, Moore CM, Khan MA, Khairuzzaman A. **A new chapter in pharmaceutical manufacturing: 3D-printed drug products**. *Advanced drug delivery reviews* 2017; 108:39-50.
9. Öblom H, Zhang J, Pimparade M, Speer I, Preis M, Repka M, et al. **3D-printed isoniazid tablets for the treatment and prevention of tuberculosis—personalized dosing and drug release**. *Aaps Pharmscitech* 2019; 20(2):1-13.
10. Bandari S, Nyavanandi D, Dumpa N, Repka MA. **Coupling Hot Melt Extrusion and Fused Deposition Modeling: Critical Properties for Successful Performance**. *Advanced Drug Delivery Reviews* 2021.
11. Melocchi A, Uboldi M, Maroni A, Foppoli A, Palugan L, Zema L, et al. **3D printing by fused deposition modeling of single-and multi-compartment hollow systems for oral delivery–A review**. *International journal of pharmaceutics* 2020; 579:119155.
12. Ong JJ, Awad A, Martorana A, Gaisford S, Stoyanov E, Basit AW, et al. **3D printed opioid medicines with alcohol-resistant and abuse-deterrent properties**. *International journal of pharmaceutics* 2020; 579:119169.
13. Lee J, Song C, Noh I, Song S, Rhee Y-S. **Hot-Melt 3D Extrusion for the Fabrication of Customizable Modified-Release Solid Dosage Forms**. *Pharmaceutics* 2020; 12(8):738.
14. Fanous M, Gold S, Muller S, Hirsch S, Ogorka J, Imanidis G. **Simplification of fused deposition modeling 3D-printing paradigm: Feasibility of 1-step direct powder printing for immediate release dosage form production**. *International journal of pharmaceutics* 2020; 578:119124.
15. Goyanes A, Allahham N, Trenfield SJ, Stoyanov E, Gaisford S, Basit AW. **Direct powder extrusion 3D printing: Fabrication of drug products using a novel single-step process**. *International journal of pharmaceutics* 2019; 567:118471.
16. Goyanes A, Chang H, Sedough D, Hatton GB, Wang J, Buanz A, et al. **Fabrication of controlled-release budesonide tablets via desktop (FDM) 3D printing**. *International journal of pharmaceutics* 2015; 496(2):414-420.

17. Pietrzak K, Isreb A, Alhnan MA. **A flexible-dose dispenser for immediate and extended release 3D printed tablets**. *European journal of pharmaceutics and biopharmaceutics* 2015; 96:380-387.
18. Cerda JR, Arifi T, Ayyoubi S, Knief P, Ballesteros MP, Keeble W, et al. **Personalised 3D printed medicines: Optimising material properties for successful passive diffusion loading of filaments for fused deposition modelling of solid dosage forms**. *Pharmaceutics* 2020; 12(4):345.
19. Okwuosa TC, Stefaniak D, Arafat B, Isreb A, Wan K-W, Alhnan MA. **A lower temperature FDM 3D printing for the manufacture of patient-specific immediate release tablets**. *Pharmaceutical research* 2016; 33(11):2704-2712.
20. Tan DK, Maniruzzaman M, Nokhodchi A. **Advanced pharmaceutical applications of hot-melt extrusion coupled with fused deposition modelling (FDM) 3D printing for personalised drug delivery**. *Pharmaceutics* 2018; 10(4):203.
21. Alhijjaj M, Belton P, Qi S. **An investigation into the use of polymer blends to improve the printability of and regulate drug release from pharmaceutical solid dispersions prepared via fused deposition modeling (FDM) 3D printing**. *European Journal of Pharmaceutics and Biopharmaceutics* 2016; 108:111-125.
22. Arafat B, Wojsz M, Isreb A, Forbes RT, Isreb M, Ahmed W, et al. **Tablet fragmentation without a disintegrant: A novel design approach for accelerating disintegration and drug release from 3D printed cellulosic tablets**. *European Journal of Pharmaceutical Sciences* 2018; 118:191-199.
23. Goyanes A, Martinez PR, Buanz A, Basit AW, Gaisford S. **Effect of geometry on drug release from 3D printed tablets**. *International journal of pharmaceutics* 2015; 494(2):657-663.
24. Goyanes A, Buanz AB, Hatton GB, Gaisford S, Basit AW. **3D printing of modified-release aminosalicylate (4-ASA and 5-ASA) tablets**. *European Journal of Pharmaceutics and Biopharmaceutics* 2015; 89:157-162.
25. Ibrahim M, Barnes M, McMillin R, Cook DW, Smith S, Halquist M, et al. **3D printing of metformin HCl PVA tablets by fused deposition modeling: drug loading, tablet design, and dissolution studies**. *AAPS PharmSciTech* 2019; 20(5):1-11.
26. Korte C, Quodbach J. **Formulation development and process analysis of drug-loaded filaments manufactured via hot-melt extrusion for 3D-printing of medicines**. *Pharmaceutical development and technology* 2018; 23(10):1117-1127.
27. Kyobula M, Adedeji A, Alexander MR, Saleh E, Wildman R, Ashcroft I, et al. **3D inkjet printing of tablets exploiting bespoke complex geometries for controlled and tuneable drug release**. *Journal of Controlled release* 2017; 261:207-215.
28. Lamichhane S, Park J-B, Sohn DH, Lee S. **Customized novel design of 3D printed pregabalin tablets for intra-gastric floating and controlled release using fused deposition modeling**. *Pharmaceutics* 2019; 11(11):564.
29. Khaled SA, Alexander MR, Irvine DJ, Wildman RD, Wallace MJ, Sharpe S, et al. **Extrusion 3D printing of paracetamol tablets from a single formulation with tunable release profiles through control of tablet geometry**. *AAPS PharmSciTech* 2018; 19(8):3403-3413.
30. Zhang B, Guo L, Chen H, Ventikos Y, Narayan RJ, Huang J. **Finite element evaluations of the mechanical properties of polycaprolactone/hydroxyapatite scaffolds by direct ink writing: Effects of pore geometry**. *Journal of the Mechanical Behavior of Biomedical Materials* 2020:103665.

31. Sadia M, Arafat B, Ahmed W, Forbes RT, Alhnan MA. **Channelled tablets: An innovative approach to accelerating drug release from 3D printed tablets**. *Journal of Controlled Release* 2018; 269:355-363.
32. Welsh NR, Malcolm RK, Devlin B, Boyd P. **Dapivirine-releasing vaginal rings produced by plastic freeforming additive manufacturing**. *International Journal of Pharmaceutics* 2019; 572:118725.
33. Nasereddin JM, Wellner N, Alhijjaj M, Belton P, Qi S. **Development of a simple mechanical screening method for predicting the feedability of a pharmaceutical FDM 3D printing filament**. *Pharmaceutical research* 2018; 35(8):151.
34. Elbadawi M, Castro BM, Gavins FK, Ong JJ, Gaisford S, Pérez G, et al. **M3DISEEN: A novel machine learning approach for predicting the 3D printability of medicines**. *International Journal of Pharmaceutics* 2020; 590:119837.
35. Scoutaris N, Ross SA, Douroumis D. **3D printed "Starmix" drug loaded dosage forms for paediatric applications**. *Pharmaceutical research* 2018; 35(2):1-11.
36. Goyanes A, Fina F, Martorana A, Sedough D, Gaisford S, Basit AW. **Development of modified release 3D printed tablets (printlets) with pharmaceutical excipients using additive manufacturing**. *International journal of pharmaceutics* 2017; 527(1-2):21-30.
37. Isreb A, Baj K, Wojsz M, Isreb M, Peak M, Alhnan MA. **3D printed oral theophylline doses with innovative 'radiator-like'design: Impact of polyethylene oxide (PEO) molecular weight**. *International journal of pharmaceutics* 2019; 564:98-105.
38. Gioumouxouzis CI, Katsamenis OL, Bouropoulos N, Fatouros DG. **3D printed oral solid dosage forms containing hydrochlorothiazide for controlled drug delivery**. *Journal of Drug Delivery Science and Technology* 2017; 40:164-171.
39. Friesen DT, Shanker R, Crew M, Smithey DT, Curatolo W, Nightingale J. **Hydroxypropyl methylcellulose acetate succinate-based spray-dried dispersions: an overview**. *Molecular pharmaceutics* 2008; 5(6):1003-1019.
40. Alhijjaj M, Nasereddin J, Belton P, Qi S. **Impact of processing parameters on the quality of pharmaceutical solid dosage forms produced by fused deposition modeling (FDM)**. *Pharmaceutics* 2019; 11(12):633.
41. Goyanes A, Kobayashi M, Martínez-Pacheco R, Gaisford S, Basit AW. **Fused-filament 3D printing of drug products: microstructure analysis and drug release characteristics of PVA-based caplets**. *International journal of pharmaceutics* 2016; 514(1):290-295.
42. McIlroy C, Olmsted PD. **Deformation of an amorphous polymer during the fused-filament-fabrication method for additive manufacturing**. *Journal of Rheology* 2017; 61(2):379-397.
43. McIlroy C, Olmsted P. **Disentanglement effects on welding behaviour of polymer melts during the fused-filament-fabrication method for additive manufacturing**. *Polymer* 2017; 123:376-391.
44. Boldyreva EV, Drebushchak V, Paukov I, Kovalevskaya YA, Drebushchak TN. **DSC and adiabatic calorimetry study of the polymorphs of paracetamol**. *Journal of thermal analysis and calorimetry* 2004; 77(2):607-623.
45. Qi S, Gryczke A, Belton P, Craig DQ. **Characterisation of solid dispersions of paracetamol and EUDRAGIT® E prepared by hot-melt extrusion using thermal, microthermal and spectroscopic analysis**. *International journal of pharmaceutics* 2008; 354(1-2):158-167.
46. D'Arcy D, Corrigan O, Healy A. **Hydrodynamic simulation (computational fluid dynamics) of asymmetrically positioned tablets in the paddle dissolution**

apparatus: impact on dissolution rate and variability. *Journal of pharmacy and pharmacology* 2005; 57(10):1243-1250.
47. D'Arcy DM, Corrigan OI, Healy AM. **Evaluation of hydrodynamics in the basket dissolution apparatus using computational fluid dynamics—dissolution rate implications**. *European journal of pharmaceutical sciences* 2006; 27(2-3):259-267.
48. McDonnell D, Redmond B, D'Arcy DM, Healy AM, Corrigan OI. **An Analysis of Drug Dissolution Rates in the USP 24 Type 2 Apparatus**. In: *PAMM: Proceedings in Applied Mathematics and Mechanics*: Wiley Online Library; 2009. pp. 691-692.